nature microbiology

LETTERS

PUBLISHED: 20 JUNE 2016 | ARTICLE NUMBER: 16077 | DOI: 10.1038/NMICROBIOL.2016.77

MicrobeJ, a tool for high throughput bacterial cell detection and quantitative analysis

Adrien Ducret*†, Ellen M. Quardokus and Yves V. Brun*

Single-cell analysis of bacteria and subcellular protein localization dynamics has shown that bacteria have elaborate life cycles, cytoskeletal protein networks and complex signal transduction pathways driven by localized proteins. The volume of multidimensional images generated in such experiments and the computation time required to detect, associate and track cells and subcellular features pose considerable challenges, especially for high-throughput experiments. There is therefore a need for a versatile, computationally efficient image analysis tool capable of extracting the desired relationships from images in a meaningful and unbiased way. Here, we present MicrobeJ, a plug-in for the open-source platform ImageJ[1]. MicrobeJ provides a comprehensive framework to process images derived from a wide variety of microscopy experiments with special emphasis on large image sets. It performs the most common intensity and morphology measurements as well as customized detection of poles, septa, fluorescent foci and organelles, determines their subcellular localization with subpixel resolution, and tracks them over time. Because a dynamic link is maintained between the images, measurements and all data representations derived from them, the editor and suite of advanced data presentation tools facilitates the image analysis process and provides a robust way to verify the accuracy and veracity of the data.

The bottleneck in the ability to perform automated, quantitative analysis of cell shape, behaviour and fluorescence patterns of high-throughput experiments is that analysis tools for extracting unbiased data efficiently from these image sets have lagged behind the technology used to collect them. This is especially true for bacterial cells, which pose additional challenges because of their size and the difficulty of distinguishing them from background particles due to their low contrast and irregular morphologies. In addition, bacterial cells often have external features such as flagella, adhesive organelles and pili that are difficult to readily detect, measure and associate with cells. To accomplish these tasks and obtain information about cellular features such as poles, external organelles and subcellular localization patterns (mid-cell or polar), while tracking these features over time and relating them to one another in meaningful ways, biologists either need to use specifically tailored analysis tools, be user savvy at applying individual algorithms, or have programming skills to extract data from images.

The software tools currently available for image analysis of bacterial cells (Supplementary Table 1) offer analysis methods that typically address some, but not all of these needs, and perform best within their specialized application areas[1–9]. The vast majority of these tools fall into MATLAB or ImageJ based solutions. Many microbiologists are familiar with the MATLAB-based program MicrobeTracker[6], which has been available for many years to perform quantitative analysis of bacterial cells. MicrobeTracker allows detailed analysis of bacterial cells, including subpixel-resolution contours, quantitative measurements of fluorescence, cell segmentation and subpixel localization of fluorescent foci. The current stand-alone implementation of MicrobeTracker, Oufti[8], has improved its ability to detect confluent cells and non-rod-shaped morphologies, handle large data sets and perform automated image analysis, and provides powerful tools for data analysis and plotting, with an easier to use graphical user interface (GUI). However, although Oufti provides the ability to change the input values used by the segmentation algorithms, understanding the meaning of these values and their effect on the resulting output requires good knowledge of signal treatment. Because MATLAB has not been developed to deal with images per se, many common features available for working with image sets in ImageJ-based programs, such as working with multiple images, selecting a region of interest (ROI), applying filters and changing look-up tables (LUT), are more difficult to accomplish in Oufti.

ImageJ-based[7] or Icy-based[10] solutions, such as Coli-Inspector[2] or BactImAS[4] provide an integrated and user-friendly approach to analyse spatiotemporal localization patterns and/or the intensity of fluorescent protein fusions in time-lapse movies, but are specific to certain tasks and/or organisms. Coli-Inspector, for instance, is based on ObjectJ, which provides an integrated platform that dynamically links user-defined objects, such as cell axes, cell diameters or constriction sites across images with their corresponding properties. With ObjectJ, the user can easily interact with the images, the user-defined objects and the associated results, and has access to interactive methods and visual inspection tools for quick elimination of artefacts. However, ObjectJ and similar tools offer a limited level of automation or rely on manual detection to delineate each cell on each micrograph.

Here, we describe MicrobeJ, an ImageJ plug-in, which offers tools dedicated to addressing the challenges posed by automatically detecting and analysing the wide variety of morphologies of bacterial cells and their associated organelles. This plug-in was optimized to handle high-throughput time-lapse microscopy experiments and deal with the obstacles described above for image analysis. MicrobeJ has an interactive GUI, including drag and drop loading of images, settings and template files, icon access to frequently used functions, hover box guidance for icon functions, and user-interactive boxes (Fig. 1 and Supplementary Movie 1). The GUI facilitates interaction between image sets, data and post-processing data representation outputs, allowing users to determine the best detection parameters and ensure accuracy. MicrobeJ can be used in conjunction with the extensive library of functions and plug-ins that have been developed over the years as practical image analysis tools for ImageJ. A comprehensive description of the software is available in the Supplementary Information.

Bacterial cell detection can be achieved from either phase contrast or fluorescence images. Using conventional thresholding techniques,

Department of Biology, Indiana University, 1001 E 3rd Street, Bloomington, Indiana 47405, USA. †Present address: Bases Moléculaires et Structurales des Systèmes Infectieux, IBCP, Université Lyon 1, CNRS, UMR 5086, 7 passage du Vercors, Lyon Cedex 07 69367, France.
*e-mail: ybrun@indiana.edu; adrien.ducret@ibcp.fr

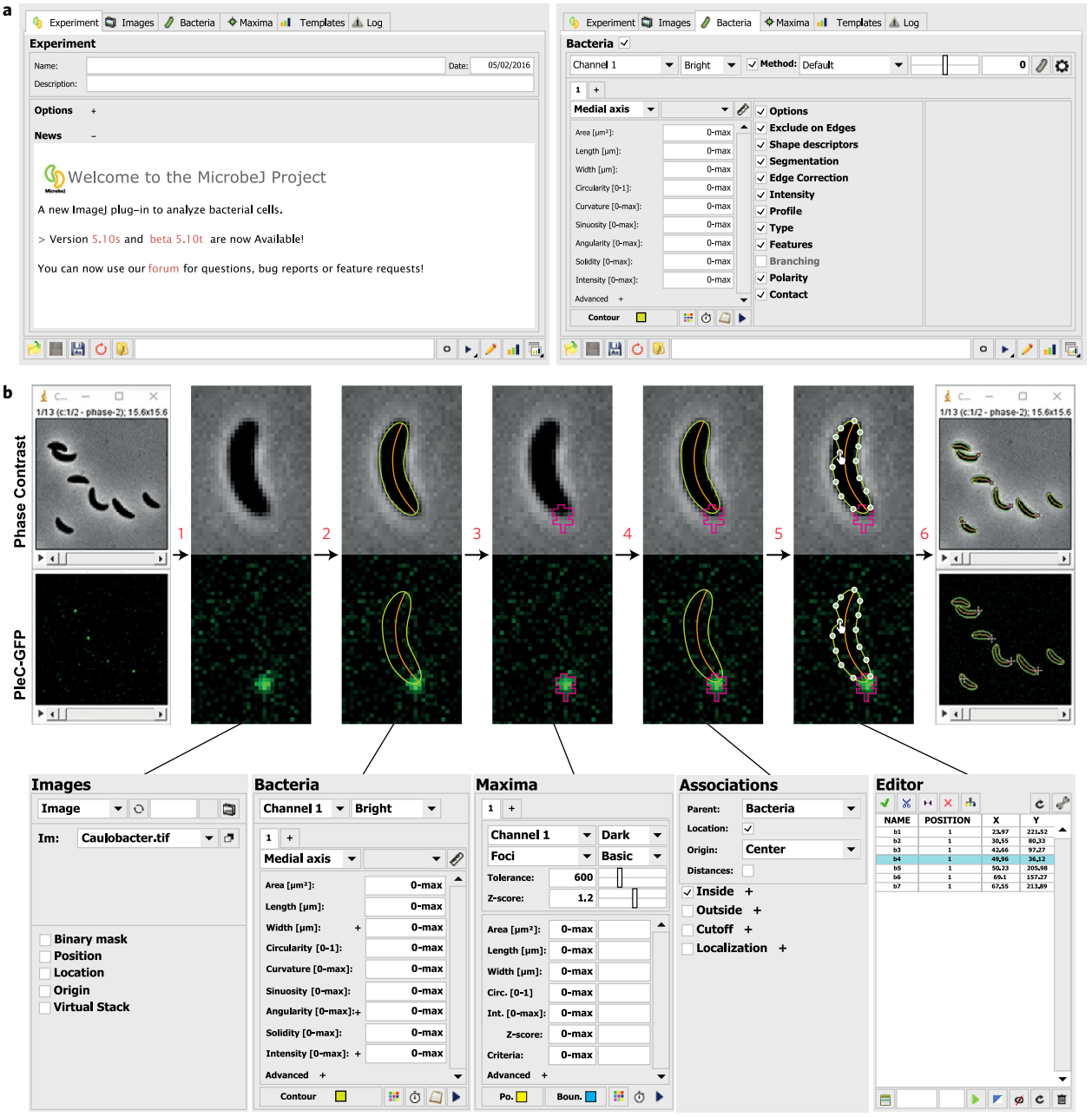

Figure 1 | The MicrobeJ GUI and workflow. a, The MicrobeJ GUI. This interface contains several tabs that allow users to set up an experiment (Experiment), select or load a set of images (Images), define parameters for bacterial cell detection and analysis (Bacteria), define parameters for fluorescent foci detection and analysis (Maxima), define and use templates (Templates), and track any errors that might arise during analysis (Log). **b**, To start, the user can simply drag and drop an image file or stack from a disk onto the MicrobeJ GUI (1), here a stack of images with *C. crescentus* cells expressing the polarly localized PleC-GFP. Once the images are loaded and selected, the user can test the bacterial cell detection settings. At any time, the user can also select dedicated options such as cell segmentation (Segmentation), fluorescence intensity measurements (Intensity), cellular type detection (Type), features detection (Feature), branched cells detection (Branching), assign poles polarity based on any particle's property (Polarity), measure the number of particles within a defined distance of the cell (Contact), or display the cell profile along a chosen axis (Profile) (2). To detect fluorescent foci, the user can test the maxima detection settings and refine further using another set of dedicated exclusion filters. The user can also select dedicated options such as the sub-pixel resolution (Gaussian Fit, not shown) or fluorescence intensity measurement (Intensity, not shown) (3). When both bacterial cells and fluorescent foci are detected, the user can associate them hierarchically using the association panel (4). At that point, the user can either manually add, edit or delete any particles detected or missed during the detection process, as in this example of a cell contour being readjusted using the active handles distributed along the polygon (5), or run the analysis on the stack of images (6) and obtain the raw data (Supplementary Fig. 4).

MicrobeJ detects particles with virtually any type of morphology and then generates subpixel resolution contours and extracts medial axes (Fig. 2a). Branched cells can be detected by selecting the 'Branching' option, whereas other shapes are automatically detected, with the ability to reject inappropriate particles based on their properties and attributes. Medial axes allow the determination of the geometrical and topological properties of the particle shape, such as its length, width, sinuosity, curvature and angularity, and establishment of the spatial information relative to the subcellular coordinate system (see below). Both the accuracy and precision of MicrobeJ measurements

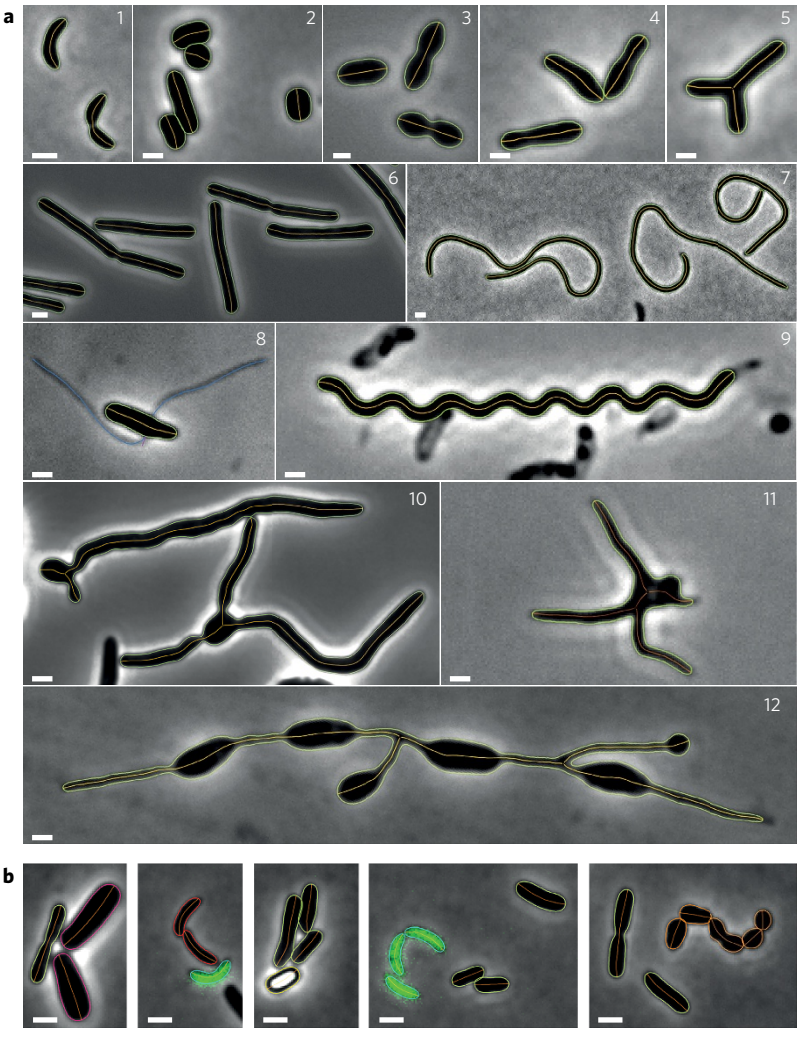

c

Type	Colour	Strain	Criteria
1		*C. crescentus*	SHAPE.width.max < 0.7 or SHAPE.sinuosity > 1.05
2		*C. crescentus* (GFP+)	SHAPE.width < 0.7 and INTENSITY.ch2 > 2,000
3		*L. lactis*	SHAPE.width.max > 0.7 and SHAPE.length < 1.6
4		*L. lactis* (Diplococcus)	SHAPE.width.max > 0.7 and SHAPE.length > 1.6 and SHAPE.length < 2.4 and FEATURE > 0
5		*B. subtilis*	SHAPE.width > 1.2
6		*B. subtilis* (Spore)	INTENSITY.ch1 > 5,000
Default		*E. coli*	

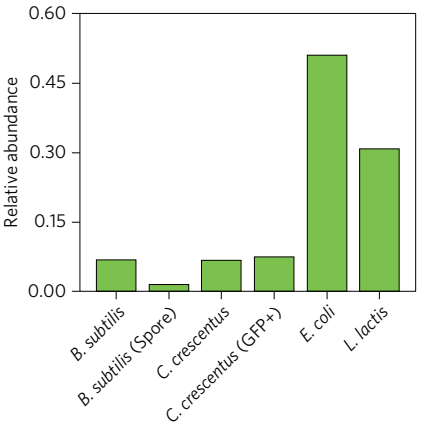

Figure 2 | MicrobeJ can detect various cell morphologies. a, Representative phase contrast images of (1) *C. crescentus* cells, (2) *S. venezuelae* cells, (3) *S. pneumoniae* cells, (4) *R. palustris* cells, (5) *A. tumefaciens* branched mutant cells, (6) *B. subtilis* cells, (7) cephalexin-treated *C. crescentus* cells, (8) *A. biprosthecum* cells, (9) two-week-old, viable, late stationary phase-adapted *C. crescentus* cells, (10) vegetative *S. venezuelae* cells, (11) long-stalked morphotype *P. hirshii* cells and (12) *Rhodomicrobium* sp. cells. The bacterial cell contours (green) and their corresponding medial axes (orange) are shown. *A. biprosthecum* stalks, detected and associated with the cell using the filament detection option, are shown in blue (8). Scale bars, 1 μm. **b**–**d**, In this experiment, *C. crescentus* CB15 cells (red contours), *C. crescentus* cells expressing a cytoplasmic green fluorescent protein (GFP) (*mini-Tn7(Gm)gfp*) (cyan contours), *B. subtilis* vegetative cells (magenta contours), *B. subtilis* spores (yellow contours), *L. lactis* cells (orange contours) and *E. coli* MG1655 cells (green contours) were mixed together and imaged on an agarose pad. Scale bars, 1 μm. Cellular types were defined using the morphological and signal properties based on the specified criteria (**c**). The relative abundance of each type is shown in **d**.

are in accordance with those reported by other cell subpixel contour detection methods[8,9] (Supplementary Fig. 1 and Supplementary Table 1; see Supplementary Section 'Bacterial cell detection').

For each particle, MicrobeJ provides a data structure that contains properties or complementary information, based on user-selected options, in the form of fields that can be accessed using an intuitive object-oriented semantic (Supplementary Table 2). For instance, the average and minimal value of width measured along the medial axis of a particle can be obtained using the semantics 'SHAPE.width.mean' and 'SHAPE.width.min', respectively. Using this terminology, particle properties can be used to define cellular types based on user-defined criteria. To demonstrate this, we mixed cells of various species with different morphologies or refractive indices and used morphological and signal properties to define six different cellular types to determine their relative abundance (Fig. 2b,c and Supplementary Fig. 2).

Options are available for processes such as feature detection (constriction, fluorescent septa or fluorescent patches) and fluorescence or width profile extraction. Using the selected options, MicrobeJ computes the specific properties and selected outputs for each particle during the detection process. Particle properties can be used to define cellular types (Fig. 2b,c), cell polarity or temporal events. To illustrate those functionalities, we analysed time-lapse images of *Caulobacter crescentus* cells harbouring FtsZ-YFP and tracked the respective localization of FtsZ and the cell constriction during the cell cycle (Fig. 3a, Supplementary Movies 2 and 3). To extract the time delay between these events and cell separation, we defined two temporal events. Temporal events consist of user-defined criteria designed to evaluate the particle properties over the time course of the experiment. When the particle meets the criteria of a specific event, the absolute and relative timing are recorded in the results table. In this example, we determined two temporal events based on the first appearance of a FtsZ-YFP fluorescent septum and a constriction, and from within MicrobeJ's results interface, plotted the distribution of their timing before division for all the cell time courses detected in this experiments (Fig. 3b).

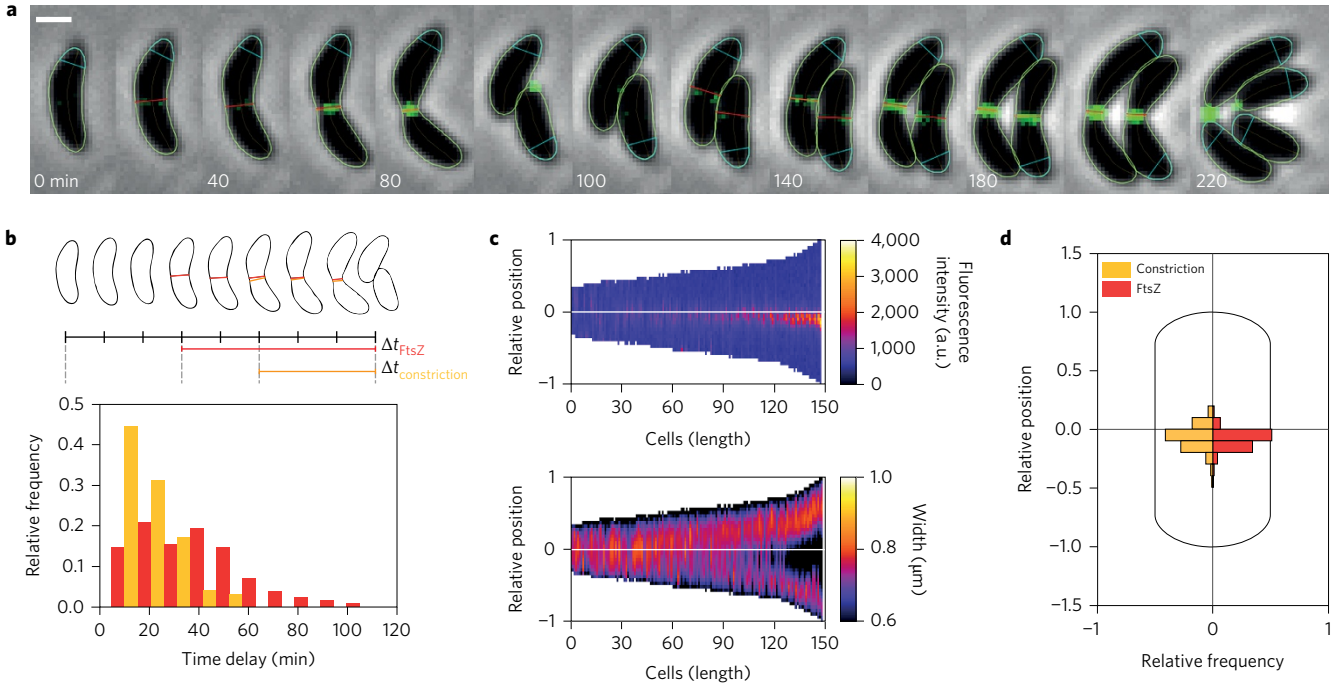

Figure 3 | Detection and quantification of the localization of FtsZ-YFP and the constriction site during the cell cycle of *C. crescentus*. All the representations depicted here are created from within the results interface of MicrobeJ. **a**, Sequence of representative phase contrast and fluorescent overlay images showing several rounds of division from a single *C. crescentus* cell expressing FtsZ-YFP. Time points are indicated for each time frame. Scale bar, 1 μm. The bacterial cell contours (green), their corresponding medial axes (orange), the position of the fluorescent septum (red) and the position of the constriction (orange) are shown. Septa were detected using the intensity profile of pixels from the fluorescent image along the medial axis of the particle. Constrictions were detected using the width profile measured along the medial axis of the particle. The orientation of the medial axis of each cell, marked by the position of the pole polygon (cyan), is determined based on the position of the constriction relative to the cell centre. **b**, Distribution of the time delay between the first appearances of the fluorescence septum (red), the constriction (orange) and cell division ($n = 352$). **c**, Demographic representation of the FtsZ-YFP fluorescence intensities and the cellular widths measured along the medial axis of the cells. Cells are sorted according to their length. The *y* axis of each demograph represents the relative position along the cell body, where 0 represents mid-cell and 1 or –1 the cell poles. The 1 pole is the pole marked by the pole polygon shown in **a**. **d**, Distribution of the localization of the septa (red) and the constriction (orange) relative to the cell centre ($n = 1,521$).

By default, the polarity of each particle is attributed randomly. However, cell polarity can be defined, based on user-defined criteria, with any geometrical and signal property (such as the width, the curvature or the fluorescence intensity) or the presence or absence of fluorescent foci or cellular features (such as constrictions or septa). The division plane in *C. crescentus* cells is asymmetrically positioned between the old-pole ('stalked') and new-pole ('swarmer')[6]. Consequently, in the example of Fig. 3, we used the relative position of the constriction site as a criterion to define the longitudinal polarity, and extracted the fluorescence and width profiles along the medial axes of the cells. The pixel intensity and the width are measured along the medial axis using the specified polarity and can be used to generate an oriented map of profiles also called a demograph (Fig. 3c). Finally, we measured the sub-cellular localization of the septa and the constrictions, and plotted their distribution relative to the centre of the cell using subcellular localization charts (Fig. 3d).

To accommodate the diverse applications requiring subcellular localization depiction, MicrobeJ provides four types of relative coordinate system (Supplementary Fig. 3a; see Supplementary Section 'Sub-cellular localization'). Each coordinate system provides specific coordinates, such as the relative position along the medial axis of the parent particle or the angle relative to the medial axis of the parent particle. These properties can be used to study the spatial distribution or the dynamics of fluorescent foci inside their parent particle using dedicated subcellular representations such as charts (Supplementary Fig. 3b) or heatmaps (Supplementary Fig. 3c). Also, when fluorescent foci or features are detected and associated with bacterial cells, the subcellular localization, the localization type and specific information (such as the number of foci per cell and their average fluorescence intensity per cell) are automatically computed for each associated particle.

Depending on the image quality, most users can simply use the software's default attribute values to detect bacterial cells with good results. In addition, MicrobeJ permits direct user interaction with the active image(s) during the detection process to optimize cell and subcellular particle detection parameters. Users can systematically change and test the settings, which may vary from experiment to experiment, before applying them to a full set of images for final analysis. In addition, the settings can be saved and applied to future image sets.

To improve the accuracy of detection in the final analysis, MicrobeJ has a comprehensive vetting system. The user can easily define a set of specific attributes referred to as 'morphology', including but not limited to area, length, width, circularity, curvature, sinuosity, angularity, solidity and signal intensity, designed to evaluate the particles in the active image. Attribute values are displayed in the image, adjacent to each detected particle. Using the attributes of particles in the image, the user can constrain the attributes in the user interface to exclude inappropriate particles or include missed particles upon re-analysis. This strategy can also be used to exclude certain particles, for example filamentous cells, from subsequent analysis. Rejected particles or groups of particles can be automatically segmented using the segmentation option. During the segmentation process, a set of methods are applied in parallel on the image in order to segment the particles. Each method

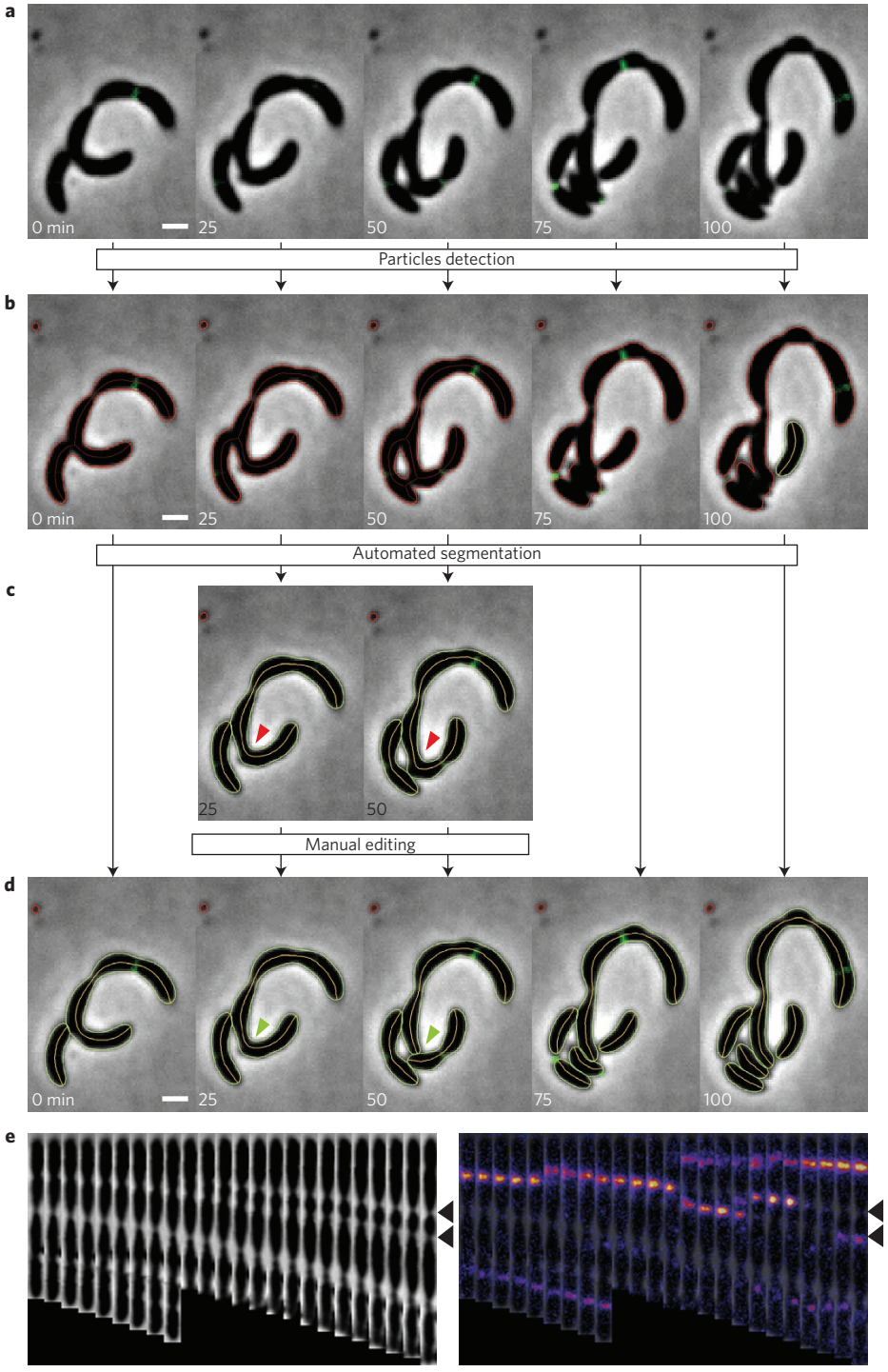

Figure 4 | Automated and manual segmentation processes. a, Sequence of representative phase contrast images showing several rounds of division from a group of *C. crescentus* cells harbouring division defects. Time points are indicated for each time frame. Scale bar, 1 µm. **b**–**d**, Particle contours computed by MicrobeJ at different steps of the segmentation process: before the automated segmentation process (**b**), after the automated segmentation process (**c**) and after manual correction (**d**). Scale bars, 1 µm. Rejected particles are shown in red, and accepted particles in green. In **c**, for clarity, the phase contrast images and their respective particle contours that did not require manual correction were hidden. Red arrows highlight the cell that needed manual segmentation. In **d**, green arrows highlight the result of manual segmentation. **e**, A montage of straightened phase contrast images (left) and fluorescence overlays showing the dynamic localization of FtsZ-YFP in a filamentous cell over time (right). Images were taken every 5 min. Black arrows highlight the two constrictions where FtsZ-YFP localizes alternately until the cell divides.

consists of specific filters (see Supplementary Section 'Bacterial cell segmentation') or user-defined ImageJ macros. For each rejected particle, the method maximizing the number of particles that meet the specified morphology attributes is chosen.

To illustrate the segmentation capabilities of MicrobeJ, we analysed a micro-colony of *C. crescentus* cells harbouring defects in cell division by time-lapse microscopy (Fig. 4a, Supplementary Movies 4 and 5). Defects in cell division can lead to poorly defined septa or randomly

localized division sites, both of which make the segmentation process more challenging (Fig. 4a,b). In this example, we optimized attribute values and used the default set of segmentation methods (see Supplementary Section 'Bacterial cell segmentation') to segment the rejected particles (Fig. 4c). Error and imprecision in the contour detection or particle segmentation are sometimes observed when particles are in close proximity to each other or when there is poor resolution. In that case, a manual correction can be performed to add, edit or delete any particles detected or missed during the automated detection process. In our example, we manually separated unsegmented cells (Fig. 4d, Supplementary Movies 4 and 5) and then generated the montage of straightened phase contrast and fluorescence images (Fig. 4e).

Once the final image analysis has been completed, MicrobeJ provides a results interface for fast data post-processing workflow and to evaluate the accuracy of the output. This interface combines information about the experiment, the detected particles and complementary data based on user-selected options (Supplementary Fig. 4a). Although particle measurements can be saved as a .csv file or copied into other programs for subsequent data analysis, the user can easily produce data representations of common statistical analyses (Supplementary Fig. 4b), interactive charts (Supplementary Fig. 4c), fluorescence map profiles (Supplementary Fig. 4d), regression analyses (Supplementary Fig. 4e) or simple custom results tables directly from within the results interface. The major advantage of data post-processing in MicrobeJ is that each row of data for a cell or focus is dynamically linked to the image and to each type of data representation derived from it. Thus, users can rapidly display subsets of data easily across all data representations. One major challenge biologists face when using automated image analysis programs lies in determining the accuracy and veracity of the data, so exploiting the dynamic link between the images, data and data representations provides an efficient strategy to verify data points and exclude any from further analysis that appear to be artefacts. Finally, the user can save the list of generated data representation outputs as a template that can be reused for future image analyses. The use of templates significantly speeds up the creation of frequently compared cellular parameter outputs, simplifying the analysis and interpretation of data without specific training in image analysis or programming (Supplementary Movie 1). Finally, a batch-processing interface allows consistent analysis across images and experiments (Supplementary Fig. 5). These features facilitate customizable, high-throughput analysis of large image data sets (see Supplementary Section 'Batch-processing').

In summary, we have shown how MicrobeJ can be used to analyse the large amounts of data contained in multidimensional image sets. MicrobeJ introduces several new features and concepts for analysing bacterial cells within a highly customizable user interface. Earlier versions of MicrobeJ were successfully used to analyse different types of bacterial cells, notably to quantify the subcellular localization patterns of a developmental regulator and morphogen in the genera *Caulobacter* and *Asticcacaulis*[11], the spatial dynamics of a versatile surface transporter in *Myxococcus xanthus*[12], as well as the dynamic subcellular localization of a respiratory complex in *Escherichia coli*[13]. MicrobeJ is supported by a detailed user's guide and video tutorials with examples, which are available on a dedicated website (http://www.indiana.edu/~microbej/) and will remain freely available and open-source. Additional functionalities will be added over time based on user feedback and new research needs, and the latest releases will be updated online. We expect that MicrobeJ will facilitate quantitative image analysis for both novices and experts in image analysis.

Methods

Bacterial strains, plasmids and growth. *Caulobacter crescentus*, *Bacillus subtilis*, *Asticcacaulis biprosthecum*, *Rhodomicrobium* sp. and *Prosthecomicrobium hirshii* were grown in peptone yeast extract (PYE)[14] at 30 °C. *Agrobacterium tumefaciens*, *Streptomyces venezuelae* and *Lactococcus lactis* were grown in Luria-Bertani (LB)[15] at 30 °C and *Escherichia coli* were grown in LB[15] at 37 °C. *M. xanthus* were grown at 32 °C in casitone yeast extract (CYE)[16]. *Streptococcus pneumoniae* were grown at 37 °C in Todd-Hewitt yeast extract (THY)[17]. *Rhodopseudomonas palustris* CGA009 was grown anaerobically in defined mineral medium (PM)[18] supplemented with 10 mM succinate and incubated at 30 °C with constant illumination from a 60 W incandescent light bulb.

Phase and fluorescence time-lapse imaging was performed on a Nikon Ti-E inverted microscope, equipped with a Plan Apo ×60, 1.40 NA, oil, Ph3 DM objective and ×1.5 magnifier. Images were acquired every 5 min, and fluorescent proteins were illuminated with a Lumencor Spectra X light engine equipped with excitation filters 470/24 (GFP), 510/25 (YFP) or 575/25 (mCherry), Chroma emission filters 510/40 (GFP), 545/30 (YFP), 530/60 (mCherry) and either a quad polychroic DAPI/FITC/Cy3/Cy5 or triple polychroic CFP/YFP/mCherry cube for Lumencor SpectraX. Images were acquired using an Andor iXon3 DU885 EM charge-coupled device camera driven by NIS Elements Advanced Research software (Nikon).

Cultures from strain YB4667 CB15::pvan-*ftsZ-yfp* were grown in PYE medium at 30 °C and induced for 2 h with 0.5 mM vanillic acid to express FtsZ-YFP. Exponentially growing cells from this culture were spotted onto a 0.8-mm-thick 1% agarose pad made with PYE medium containing 0.5 mM vanillic acid, and time-lapse images were acquired every 5 min from 16 different slide positions for 54 time points. For cell division inhibition, 30 μg ml^{-1} cephalexin was added to the agarose pad during the imaging period.

For precision assessment of MicrobeJ, Molecular Probes FluoSpheres carboxylate-modified microspheres (F8823, 1 ± 0.0480 μm, lot #1761288) were spotted onto a 1% agarose pad made with deionized water, and images were acquired for 30 ms using the same microscope, camera and objective as used for the cells.

Received 13 August 2015; accepted 27 April 2016; published 20 June 2016

References

1. Schneider, C.A., Rasband, W.S. & Eliceiri, K. W. NIH image to ImageJ: 25 years of image analysis. *Nature Methods* **9,** 671–675 (2012).
2. Vischer, N. O. E. *et al.* Cell age dependent concentration of *Escherichia coli* divisome proteins analyzed with ImageJ and ObjectJ. *Front. Microbiol.* **6,** 586 (2015).
3. Liu, J., Dazzo, F. B., Glagoleva, O., Yu, B. & Jain, A. K. CMEIAS: a computer-aided system for the image analysis of bacterial morphotypes in microbial communities. *Microb. Ecol.* **41,** 173–194 (2001).
4. Mekterović, I., Mekterović, D. & Maglica, Z. BactImAS: a platform for processing and analysis of bacterial time-lapse microscopy movies. *BMC Bioinformatics* **15,** 251 (2014).
5. Christen, B. *et al.* High-throughput identification of protein localization dependency networks. *Proc. Natl Acad. Sci. USA* **107,** 4681–4686 (2010).
6. Sliusarenko, O., Heinritz, J., Emonet, T. & Jacobs-Wagner, C. High-throughput, subpixel precision analysis of bacterial morphogenesis and intracellular spatio-temporal dynamics. *Mol. Microbiol.* **80,** 612–627 (2011).
7. Schindelin, J. *et al.* Fiji: an open-source platform for biological-image analysis. *Nature Methods* **9,** 676–682 (2012).
8. Paintdakhi, A. *et al.* Oufti: an integrated software package for high-accuracy, high-throughput quantitative microscopy analysis. *Mol. Microbiol.* **99,** 767–777 (2016).
9. Guberman, J. M., Fay, A., Dworkin, J., Wingreen, N. S. & Gitai, Z. PSICIC: noise and asymmetry in bacterial division revealed by computational image analysis at sub-pixel resolution. *PLoS Comput. Biol.* **4,** e1000233 (2008).
10. de Chaumont, F. *et al.* Icy: an open bioimage informatics platform for extended reproducible research. *Nature Methods* **9,** 690–696 (2012).
11. Jiang, C., Brown, P. J. B., Ducret, A. & Brun, Y. V. Sequential evolution of bacterial morphology by co-option of a developmental regulator. *Nature* **506,** 489–493 (2014).
12. Wartel, M. *et al.* A versatile class of cell surface directional motors gives rise to gliding motility and sporulation in *Myxococcus xanthus*. *PLoS Biol.* **11,** e1001728 (2013).
13. Alberge, F. *et al.* Dynamic subcellular localization of a respiratory complex controls bacterial respiration. *eLife* **4,** e05357 (2015).
14. Ely, B. Genetics of *Caulobacter crescentus*. *Methods Enzymol.* **204,** 372–384 (1991).
15. Miller, J. H., Ippen, K., Scaife, J. G. & Beckwith, J. R. The promoter–operator region of the lac operon of *Escherichia coli*. *J. Mol. Biol.* **38,** 413–420 (1968).
16. Bustamante, V. H., Martínez-Flores, I., Vlamakis, H. C. & Zusman, D. R. Analysis of the Frz signal transduction system of *Myxococcus xanthus* shows the importance of the conserved C-terminal region of the cytoplasmic chemoreceptor FrzCD in sensing signals. *Mol. Microbiol.* **53,** 1501–1513 (2004).
17. Todd, E. W. & Hewitt, L. F. A new culture medium for the production of antigenic streptococcal hæmolysin. *J. Pathol. Bacteriol.* **35,** 973–974 (1932).
18. Kim, M.-K. & Harwood, C. S. Regulation of benzoate-CoA ligase in *Rhodopseudomonas palustris*. *FEMS Microbiol. Lett.* **83,** 199–203 (1991).

Acknowledgements

The authors thank all members of the Brun laboratory for many discussions. In particular, the authors thank B. LaSarre and C. Ellison for useful feedback about MicrobeJ and D. Kysela and L. Espinosa for discussions and reading the manuscript. The authors thank S. Schlimpert, N. Feirer, C. Grangeasse, T. Doan, P. Brown and B. LaSarre for providing images from *S. venezuelae* cells, *A. tumefaciens*, *S. pneumoniae*, *B. subtilis*, *P. hirshii* and *R. palustris*, respectively. The authors thank M. Thanbichler for the *pvan-ftsZ-yfp* carrying the *Caulobacter* strain. This research was supported by National Institutes of Health grants GM51986 and GM113172, and by seed funding from the Indiana University Office of the Vice-President for Research. This project was supported, in part, by the Indiana Clinical and Translational Sciences Institute funded, in part, by grant UL1TR001108 from the National Institutes of Health, National Center for Advancing Translational Sciences, Clinical and Translational Sciences Award.

Author contributions

A.D. wrote the ImageJ plugin. A.D. and Y.V.B. planned the project. A.D. and E.M.Q. performed the experiments. A.D., E.M.Q. and Y.V.B. analysed the data. A.D., E.M.Q. and Y.V.B. wrote the paper.

Additional information

Supplementary information is available online. Reprints and permissions information is available online at www.nature.com/reprints. Correspondence and requests for materials should be addressed to A.D. and Y.V.B.

Competing interests

The authors declare no competing financial interests.